Biochemical and Biophysical Research Communications 452 (2014) 992–997

Contents lists available at ScienceDirect

Biochemical and Biophysical Research Communications

journal homepage: www.elsevier.com/locate/ybbrc

Insights in $K_{IR}2.1$ channel structure and function by an evolutionary approach; cloning and functional characterization of the first reptilian inward rectifier channel $K_{IR}2.1$, derived from the California kingsnake (*Lampropeltis getula californiae*)

Marien J.C. Houtman [a,*], Sanne M. Korte [a], Yuan Ji [a], Bart Kok [a], Marc A. Vos [a], Anna Stary-Weinzinger [b], Marcel A.G. van der Heyden [a]

[a] Department of Medical Physiology, DH&L, UMC Utrecht, The Netherlands
[b] Department of Pharmacology and Toxicology, University of Vienna, Vienna, Austria

ARTICLE INFO

Article history:
Received 28 August 2014
Available online 16 September 2014

Keywords:
$K_{IR}2.1$
Ion channel
Electrophysiology
Molecular modelling
Phylogeny
Andersen–Tawil disease

ABSTRACT

Potassium inward rectifier $K_{IR}2.1$ channels contribute to the stable resting membrane potential in a variety of muscle and neuronal cell-types. Mutations in the $K_{IR}2.1$ gene *KCNJ2* have been associated with human disease, such as cardiac arrhythmias and periodic paralysis. Crystal structure and homology modelling of $K_{IR}2.1$ channels combined with functional current measurements provided valuable insights in mechanisms underlying channel function. $K_{IR}2.1$ channels have been cloned and analyzed from all main vertebrate phyla, except reptilians. To address this lacuna, we set out to clone reptilian $K_{IR}2.1$ channels. Using a degenerated primer set we cloned the *KCNJ2* coding regions from muscle tissue of turtle, snake, bear, quail and bream, and compared their deduced amino acid sequences with those of $K_{IR}2.1$ sequences from 26 different animal species obtained from Genbank. Furthermore, expression constructs were prepared for functional electrophysiological studies of ectopically expressed $K_{IR}2.1$ ion channels. In general, *KCNJ2* gene evolution followed normal phylogenetic patterns, however turtle $K_{IR}2.1$ ion channel sequence is more homologues to avians than to snake. Alignment of all 31 $K_{IR}2.1$ sequences showed that all disease causing $K_{IR}2.1$ mutations, except V93I, V123G and N318S, are fully conserved. Homology models were built to provide structural insights into species specific amino acid substitutions. Snake $K_{IR}2.1$ channels became expressed at the plasmamembrane and produced typical barium sensitive (IC_{50} ~6 μM) inward rectifier currents.

1. Introduction

Inward rectifier channels [1] conduct potassium ions, depending on the membrane potential, either into or out of cells. In general, inward currents are larger than outward currents at similar deviations negative or positive, respectively, from the potassium equivalent potential. The human genome harbors sixteen inward rectifier genes that code for seven subfamilies of inward rectifier channels, named $K_{IR}1$-7, which become expressed in many different tissues and organs [2]. In vertebrate species, inward rectifier potassium channels of the $K_{IR}2.x$ family fulfill an important role in setting the resting membrane potential of excitable cells. In the mammalian heart, inward rectifier channels of the $K_{IR}2.x$ family, coded by the *KCNJ2* ($K_{IR}2.1$), *KCNJ4* ($K_{IR}2.3$) and *KCNJ12* ($K_{IR}2.2$) genes, are responsible for the stable and negative resting membrane potential at approximately −80 mV between action potentials and are also involved in phase 3 repolarization. Mammalian skeletal muscle expresses *KCNJ2, KCNJ12* and *KCNJ18* ($K_{IR}2.6$) whereas also smooth muscle cells show functional $K_{IR}2.1$, 2.2, 2.3 and 2.4 expression. Furthermore, members of the $K_{IR}2.x$ family become expressed in neural cells, the eye, placenta and kidney cells (reviewed in [2]).

Inward rectifier inhibition in humans due to barium intoxication results in a plethora of clinical symptoms mostly affecting cardiac, skeletal and smooth muscle systems and resulting in, amongst others, vomiting, diarrhea, muscle paralysis and cardiac

Abbreviations: ATS1, Andersen–Tawil syndrome 1; *Bb*, *Blicca bjoerkna*; *Hs*, *Homo sapiens*; *Lg*, *Lampropeltis getula californiae*; *Tse*, *Trachemys scripta elegans*.

* Corresponding author at: Department of Medical Physiology, DH&L, Yalelaan 50, 3584 CM Utrecht, The Netherlands. Fax: +31 30 2539036.
E-mail address: M.J.C.Houtman@umcutrecht.nl (M.J.C. Houtman).

http://dx.doi.org/10.1016/j.bbrc.2014.09.031
0006-291X/

arrhythmias [3]. More specific impairments of human $K_{IR}2.1$ function have been found in the very rare Andersen–Tawil Syndrome 1 (ATS1), that associates with *KCNJ2* loss-of-function mutations that can result in ventricular arrhythmias, periodic paralysis, with or without hypokalemia, and dysmorphic features [4]. Currently, approximately 70 different mutations, mostly missense, have been identified that are located in many different functional regions of the protein (reviewed in [5]). In contrast, only a few gain-of-function mutations have been found today that are either associated with atrial fibrillation and short QT-syndrome [5].

Mechanistic insights into inward rectifier channel function has benefited enormously from X-ray structures of bacterial and eukaryotic K_{IR} channels, including $K_{IR}2.x$ channels [6–11]. Obviously, upon close inspection structural differences between the prokaryotic and mammalian homologues are evident and have been linked to functional behavior with respect to lipid dependent inhibition and activation, respectively [12]. Apart from crystallization studies, homology modelling approaches [13] has revealed another wealth of information on $K_{IR}2.1$ channel structure-function relationships [14–17]. Furthermore, homology models are very useful to simulate drug-channel interactions and both development of new compounds and drug-safety predictions are key applications [18,19]. In general, an in silico protein model of a given protein is built on basis of its homology with proteins from which crystal structures have been revealed, and as such it is a very powerful tool for those ion channels for which crystal structure information is hard to obtain due to experimental limitations. In this field, cross-species homology is an important factor since the degree of homology has a direct impact on the quality of the model [20].

The first mammalian $K_{IR}2.1$ channel was cloned in the early 1990s from mouse [21], and cloning and functional analysis of $K_{IR}2.1$ channels from other vertebrate phyla followed [22,23]. As of to date, *KCNJ2* has been cloned and functionally analyzed from all main vertebrate phyla, except from that of reptilians. To enable a comprehensive vertebrate cross-phyla comparison of *KCNJ2* coding sequences and link this analysis with current knowledge on $K_{IR}2.1$ function and human *KCNJ2* mutations, we set out to clone reptilian *KCNJ2* coding regions and analyze resulting $K_{IR}2.1$ channels' functional properties.

2. Materials and methods

2.1. Tissue

California kingsnake (*Lampropeltis getula californiae; Lg*) heart and Red-eared Slider (*Trachemys scripta elegans; Tse*) skeletal muscle were obtained from Dr. Marja J.L. Kik (Dept of Veterinary Pathology, Faculty of Veterinary Medicine, Utrecht University, The Netherlands). American black bear (*Ursus americanus; Ua*) heart was obtained as described earlier [24]. White bream (*Blicca bjoerkna*; *Bb*) heart was obtained from a local fisherman from the Tiel area (Netherlands). Japanese quail (*Coturnix japonica; Cj*) heart was obtained from a local quail breeding farm (Dirk de Jong, IJsselstein, The Netherlands).

2.2. Cloning of KCNJ2

Total RNA was isolated from a piece of tissue using Trizol (Invitrogen, Breda, The Netherlands) according to the manufacturers recommendations, and preparations were treated with DNase. cDNA was made using oligo-dT and Superscript II (Invitrogen). Subsequently, *KCNJ2* was amplified by PCR in triplo, using a mixture of sense and antisense primers based on mouse, chicken, *Xenopus* and zebrafish *KCNJ2* sequences (sense, GTGATGGGCAGCGTGCG AACCAACC (chicken/Xenopus), GCGATGGGCAGTGTGAGAACCAACC (mouse), GTGATGGGAAGTGTGCGGGCCAACC (zebrafish); antisense, AGTCATATTTCAGATTCTCGCC (zebrafish/Xenopus), AGTCATATTTCCGACTCACGCC (chicken), AGTCATATCTCCGATTCTCGCC (mouse)). PCR products were run on a ethidium bromide stained 1% agarose gel, excised and cloned in pGEM-T-easy (Promega) and sequenced as described previously [25]. The three independent sequences were compared to exclude PCR based artefacts.

2.3. Sequence analysis and phylogeny

Alignment and phylogenetic tree reconstruction was performed with MEGA version 4.0 software [26] operating with ClustalW and Neighbor-Joining algorithms. Support for each node was determined by interior-branch test (1000 replicates; seed = 64238).

2.4. Molecular modelling

A homology model of the transmembrane domain of the human $K_{IR}2.1$ channel was built using Modeller 9v9 with the $K_{IR}2.2$ crystal structure (pdb identifier: 3spi, [10]) as template, which shares 70% sequence identity with $K_{IR}2.1$. The crystal structure of the cytoplasmic domain of $K_{IR}2.1$ from *Mus musculus* (pdb identifier: 1u4f, [7]) served as template for generation of the human C-terminal domain structure. Due to very high sequence identity >90%, the *Bb*$K_{IR}2.1$ channel model was obtained by in silico replacement of the species specific residues in the *Hs*$K_{IR}2.1$ model. Figures were generated with Pymol.

2.5. Ectopic expression and detection of snake $K_{IR}2.1$ by immunofluorescence microscopy and Western blot

Validated Californian kingsnake sequence was subcloned in pcDNA3 vector to generate the *Lg*$K_{IR}2.1$ expression construct. COS-7 cells were subsequently used for *Lg*$K_{IR}2.1$ protein detection by immunofluorescence microscopy (antibody: sc-28633, Santa Cruz Biotechnology) and western blot respectively (antibody: sc-18708, Santa Cruz Biotechnology, Dallas, TX, USA). Immunofluorescence microscopy was performed as described earlier [27]. Sodium dodecyl sulphate-polyacrylamide gel electrophoresis (SDS-PAGE) was performed as described previously [28].

2.6. Electrophysiology

HEK293 cells cultured on glass coverslips were co-transfected with 1.0 μg pcDNA–*Lg*$K_{IR}2.1$ and 0.5 μg pEGFP-1 expression constructs. Patch clamp measurements were done as described before [28] using an AxoPatch 200B amplifier controlled by pClamp9 software (Molecular devices, Sunnyvale, CA, USA). Whole cell $I_{KIR2.1}$ measurements were performed by applying 1s test pulses ranging between −120 and + 30 mV, in 10 mV increments, from a holding potential of −40 mV, and with series resistance compensation of at least 70%. Steady state current at the end of the pulse was normalized to cell capacitance and plotted versus test potential (corrected for liquid junction potential). Extracellular solution contained (in mmol/L): NaCl 140, KCl 5.4, $CaCl_2$ 1, $MgCl_2$ 1, glucose 6, $NaHCO_3$ 17.5, HEPES 15, pH7.4/NaOH. Pipette solution contained potassium gluconate 125, KCl 10, HEPES 5, EGTA 5, $MgCl_2$ 2, $CaCl_2$ 0.6, Na_2ATP 4, pH7.20/KOH. Hill fitting for $BaCl_2$ IC_{50} estimation was carried out using Graphpad Prism version 6.0c (Graphpad, La Jolla, CA, USA).

3. Results and discussion

3.1. Cloning of reptilian $K_{IR}2.1$

To obtain new *KCNJ2* cDNAs from vertebrate species, we applied an RT-PCR based approach on muscle tissue derived RNA using a

degenerated primer set based on known *KCNJ2* sequence of four vertebrate species (*Mus musculus*, *Gallus gallus*, *Xenopus tropicalis*, *Danio rerio*) similar as for cloning of complete open reading frame *GJA1* sequences [25]. Complete open reading frame *KCNJ2* cDNA was amplified and cloned from snake (*Lg*, *Lampropeltis getula californiae*; California kingsnake; Accession number KM261808) and turtle (*Tse*, *Trachemys scripta elegans*; Red-eared slider; KM261809) (Fig. 1). Snake and turtle $K_{IR}2.1$ amino acid sequences were approximately 93% and 95% identical to human $K_{IR}2.1$, respectively. Using an identical approach, additional complete *KCNJ2* open reading frame sequences were cloned from fish (*Bb*, *Blicca bjoerkna*; White bream; KM261812), bear (*Ua*, *Ursus americanus*; American black bear; KM261811) and bird (*Cj*, *Coturnix japonica;* Japanese quail; KM261810). For each species, three independent clones were sequenced in both directions. Unfortunately, using this primer set we were unable to amplify shark (*Scyliorhinus canicula*) *KCNJ2* sequences from heart, skeletal muscle or brain tissue cDNA or genomic DNA.

3.2. Sequence comparison of vertebrate $K_{IR}2.1$ reveals strong homology in structural, trafficking, interaction domains and in most human disease associated mutations

Next, deduced amino acid sequences from our newly cloned $K_{IR}2.1$ were aligned with 26 $K_{IR}2.1$ protein sequences derived from literature and various genome sequencing projects (Supplemental Fig. 1). Amino acid alignment depicted large stretches of identity between $K_{IR}2.1$ from all 31 species ranging from fish to placental mammals. Many of these clusters corresponded with identified structural and functional units like transmembrane regions, slide helix, pore helix, G-loop, golgi and ER export domains [7,8,29,30]. With respect to the selectivity filter region, two fish specific substitutions were observed (F147Y and C149Y, numbering according to *Hs*$K_{IR}2.1$). Currently, missense mutations at 41 different positions in human *KCNJ2* have been associated with ATS1, catecholaminergic polymorphic ventricular tachycardia, atrial fibrillation type 3 and short QT syndrome 3 [5]. With the exception of 3 missense mutation, these were all confined to regions of complete identity between the 31 different species. Of interest, V93I has been identified in short QT syndrome 3 patients [31] and the mutation results in increased current density. V93 was found not to be conserved. Interestingly, in horse, birds, reptiles and *Xenopus* an I residue is located at this position, identical as reported in the SQT patients of Xia et al. [31]. V123G is associated with ATS1 [32]. V123 was found to be conserved between all species except pufferfish (Fugu), in which it is replaced by I. Finally, the mild loss-of-function mutation N318S is associated with ATS1 [33]. N318 was found to be conserved among mammals, birds and reptiles, whereas in amphibian it is replaced by an S residue, and in some fish it is replaced by S (white bream, common carp, rainbow trout) or D (pufferfish/Fugu).

The PDZ interaction domain (ESEI) [34] at the extreme C-terminus of all aligned $K_{IR}2.1$ channel proteins was found to be conserved. However, since our cloning strategy relied on a primer directed to this region, we cannot definitely state that the two reptilian, white bream, American black bear and Japanese quail possess this conserved ESEI sequence too, but given the absolute level of conservation between the other twenty-six $K_{IR}2.1$ proteins at this position among the different phyla, it is highly likable. Furthermore, the success of our cloning approach relied on conservation of this region within the *KCNJ2* gene.

3.3. Molecular modelling of the human and fish selectivity filter, and non-conserved diseased associated mutations

Homology models were used to gain more insight into the non-conserved residues of the pore-domain region of fish and the non-conserved disease associated mutations as described in the previous section.

Homology models of the transmembrane domain of *Hs*$K_{IR}2.1$ (shown in Fig. 2A) and *Bb*$K_{IR}2.1$ were constructed using the closed $K_{IR}2.2$ crystal structure with bound PIP_2 [10]. The crystal structure of the $K_{IR}2.1$ channel from mouse served as template to build the cytoplasmic domains. Fig. 2B and C illustrates the location of the two fish specific substitutions F147Y and C149Y, located at the extracellular side of the selectivity filter. The homology model of *Bb*$K_{IR}2.1$ shows that replacement of a C with Y in position 149 enables favorable pi-pi stacking interactions with Y147 from the neighbouring subunit.

Of special interest are amino acid changes that lead to disease phenotypes. Fig. 2D and E illustrates the location of residues V93 and V123 in the *Hs*$K_{IR}2.1$ homology model. V93 is located on the

```
Lg  MGSVRANRYSIVSSEEDGMKLATMAVANGFGNGKSKVHTRQQCRSRFVKKDGHCNVQFINVGEKGQRYLADIFTTC  76
Tse MGSVRTNRYSIVSSEEDGMKLATMAVANGFGNGKSKVHTRQQCRSRFVKKDGHCNVQFINVGEKGQRYLADIFTTC  76
Hs  MGSVRTNRYSIVSSEEDGMKLATMAVANGFGNGKSKVHTRQQCRSRFVKKDGHCNVQFINVGEKGQRYLADIFTTC  76

Lg  VDIRWRWMLLIFCLAFLLSWLFFGCVFWLIALLHGDLEE--TDKPCVSEVRSFTAAFLFSIETQTTIGYGFRCVTD 150
Tse VDIRWRWMLVIFCLAFLLSWLFFGCVFWLIALLHGDLEDSGNYKPCVSNVNSFTAAFLFSIETQTTIGYGFRCVTD 152
Hs  VDIRWRWMLVIFCLAFVLSWLFFGCVFWLIALLHGDLDASKEGKACVSEVNSFTAAFLFSIETQTTIGYGFRCVTD 152

Lg  ECPIAVFMVVFQSIVGCIIDAFIIGAVMAKMAKPKKRNETLIFSHNAVVAMRDGKLCLMWRVGNLRKSHLVEAHVR 226
Tse ECPIAVFMVVFQSIVGCIIDAFIIGAVMAKMAKPKKRNETLVFSHNAVVGIRDGKLCLMWRVGNLRKSHLVEAHVR 228
Hs  ECPIAVFMVVFQSIVGCIIDAFIIGAVMAKMAKPKKRNETLVFSHNAVIAMRDGKLCLMWRVGNLRKSHLVEAHVR 228

Lg  AQLLKSRITTEGEYIPLDQIDINVGFDSGIDRIFLVSPITIVHEIDEESPLYDLSKQDMDNADFEIVVILEGMVEA 302
Tse AQLLKSRVTSEGEYIPLDQIDINVGFDSGIDRIFLVSPITIVHEIDEQSPLYDYSKQDMDNADFEIVVILEGMVEA 304
Hs  AQLLKSRITSEGEYIPLDQIDINVGFDSGIDRIFLVSPITIVHEIDEDSPLYDLSKQDIDNADFEIVVILEGMVEA 304

Lg  TAMTTQCRSSYLSNEILWGHRYEPVLFEEKNYYKVDYSRFHKTYEVPNTPLCSARDLAEKKYILSNANSFCYENEV 378
Tse TAMTTQCRSSYLANEILWGHRYEPVLFEEKNYYKVDYSRFHKTYEVPNTPLCSARDLAEKKYILSNANSFCYENEV 380
Hs  TAMTTQCRSSYLANEILWGHRYEPVLFEEKHYYKVDYSRFHKTYEVPNTPLCSARDLAEKKYILSNANSFCYENEV 380

Lg  ALAGKEEEDSDNGVPESTSTDTHPEMDHLSQAGVPLEPRPLRRESEI                              425
Tse ALTSKEEDESDNGVPESMSTDTLPDMDHHNQAGVPLEPRPLRRESEI                              427
Hs  ALTSKEEDDSENGVPESTSTDTPPDIDLHNQASVPLEPRPLRRESEI                              427
```

Fig. 1. Amino acid alignment of snake (*Lg*; California kingsnake, *Lampropeltis getula californiae*), turtle (*Tse*; Red-eared slider, *Trachemys scripta elegans*) and human (*Hs*) $K_{IR}2.1$ amino acid sequences in single letter code. Non-identical residues with respect to the human sequence are depicted in white font on a black background. Transmembrane region 1 and 2 are underlined in the human sequence. Gray shaded sequences depict the Golgi en endoplasmatic reticulum export sequences [29,30], respectively. The potassium selectivity filter is indicated in bold and italic.

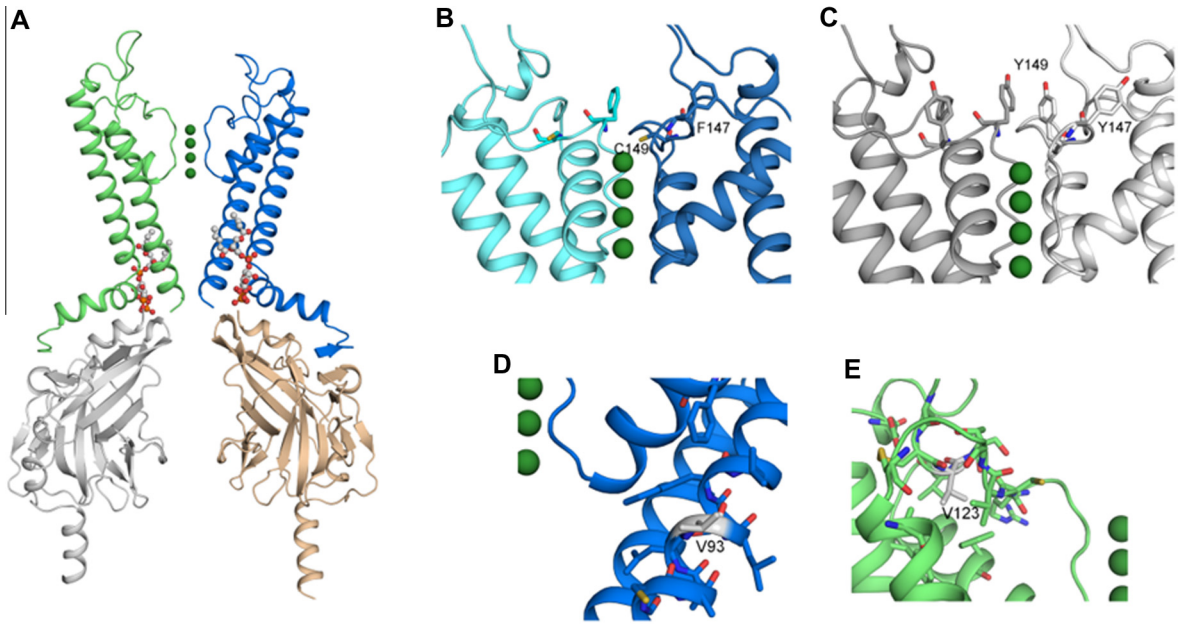

Fig. 2. Molecular modelling. (A) Homology model of *Hs*K_{IR}2.1. Two opposing subunits are shown in side view. K^+ ions are shown as green spheres; short-chain PIP_2 molecules are depicted in ball and stick representation. (B and C) Comparison of the selectivity filter regions of *Hs*K_{IR}2.1 (B) and *Bb*K_{IR}2.1 channels (C). (D) The location of V93 in the outer (M1) helix is shown as grey sticks. (E) The location of V123 behind the selectivity filter is shown (grey sticks). (For interpretation of the references to colour in this figure legend, the reader is referred to the web version of this article.)

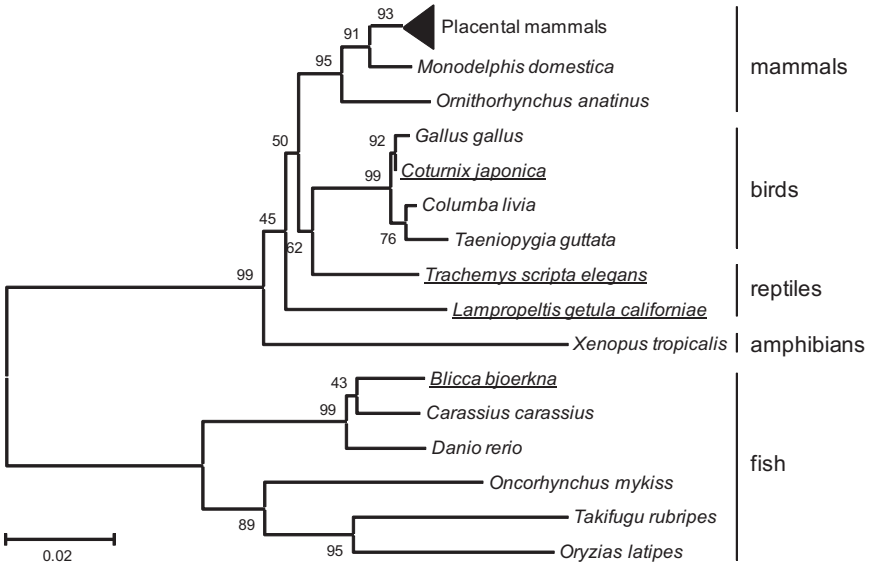

Fig. 3. Cladogram of K_{IR}2.1 sequences. The amino acid sequences of 31 K_{IR}2.1 from mammals, fish, amphibian, reptiles and birds were analyzed using MEGA software. Genbank accession numbers are defined in the legend of Supplemental Fig. 1. K_{IR}2.1 sequences derived in the current study are indicated by underlining of the species name (except American black bear that is placed in the placental mammal group). Sixteen placental animals (bovine, dog, guinea pig, armadillo, small Madagascar hedgehog, horse, human, little brown bat, rhesus monkey, mouse, European rabbit, chimpanzee, Norwegian rat, thirteenlined ground squirrel, pig and American black bear, accession numbers provided in the legend of Supplemental Fig. 1) were closely clustered and are depicted as one group for clarity. The scale bar beneath the tree measures distance between the sequences, and units indicate the number of substitution events. Support for each node (numbers) was determined by interior-branch test.

outer transmembrane helix, surrounded by hydrophobic residues and accessible to the lipid membrane. It is remarkable that a subtle change in size and hydrophobicity causes such a strong phenotype. As shown in Fig. 2E, V123 is located in a mainly hydrophobic pocket behind the selectivity filter. Replacing this amino acid with the small and flexible G, might destabilize the selectivity filter structure. The location of ATS1 mutant N318S was shown previously [33]. This residue is located on the surface of the C-terminal domain, in a 310-helix, between β-sheets I and J. It is possible that this residue interacts with the N-terminus of the adjacent subunit. Unfortunately the first 30–40 residues are missing in all currently available K_{IR} X-ray structures, thus a direct interaction of residue N318S with this segment remains hypothetical.

3.4. Phylogenetic reconstruction

Phylogenetic reconstruction analysis based on the deduced amino acid sequences (Fig. 3) indicated that in general K_{IR}2.1 evo-

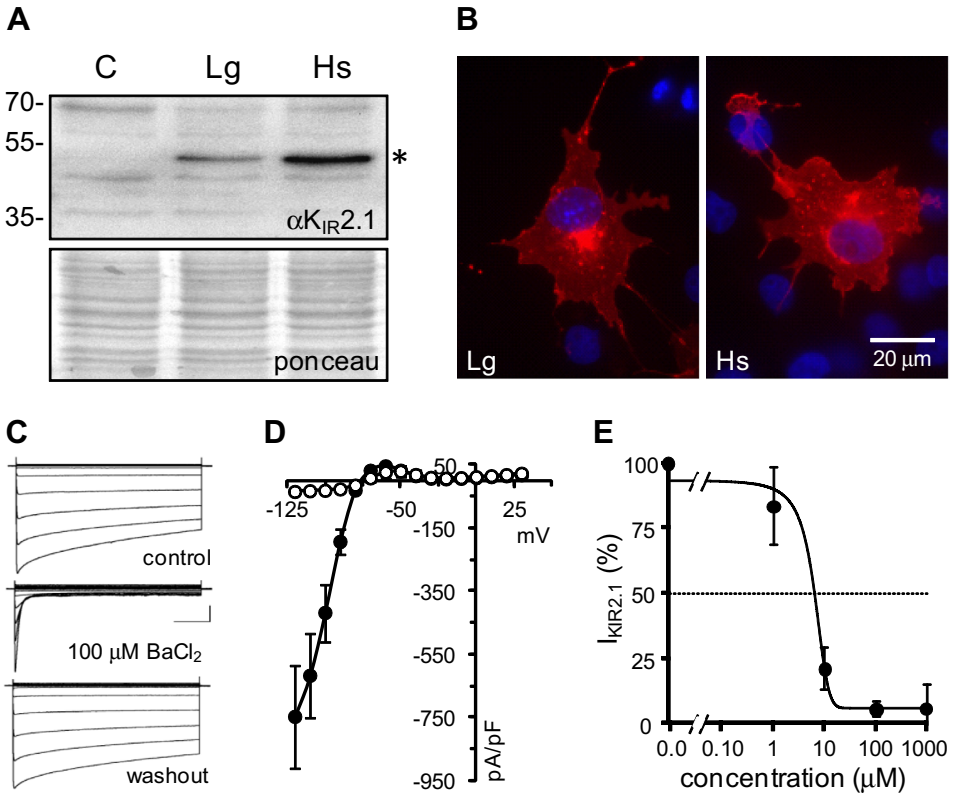

Fig. 4. Expression and electrophysiological analysis of *Lg*K_{IR}2.1. (A) *Lg*K_{IR}2.1 and *Hs*K_{IR}2.1 were transiently expressed in COS-7 cells. Whole cell lysates were separated on 10% SDS-PAGE and resulting western blots were probed for K_{IR}2.1 expression. Snake and human K_{IR}2.1 protein expression is observed with an apparent M_w of 55 kDa (indicated with *). Whole lysate ponceau S staining is used as loading control. (B) Upon transient expression of snake (Lg) and human (Hs) in COS-7 cells channel protein staining (red) is observed at the plasma membrane and membrane ruffles, and intracellularly in endoplasmic reticulum- and Golgi-like structures. Nucleus is stained blue. (C) Representative current traces of snake $I_{KIR2.1}$ recorded from transiently expressed HEK293 cells at control, 100 μM $BaCl_2$ and washout conditions as indicated. Scale bars: horizontal = 200 ms, vertical = 1000 pA. (D) Current–voltage relation curve of snake K_{IR}2.1 at control (closed symbols) and 100 μM $BaCl_2$ (open symbols) conditions (mean ± s.e.m.; control n = 9, $BaCl_2$ n = 7). (E) IC_{50} curve of $BaCl_2$ dependent inhibition of the inward component of *Lg*K_{IR}2.1 current at −120 mV (mean ± s.d.; n = 5–9, for each concentration). (For interpretation of the references to colour in this figure legend, the reader is referred to the web version of this article.)

lution follows vertebrate evolutionary pathways. The reptilian K_{IR}2.1 sequences became positioned between the clades of amphibian and birds, thereby filling the previous existing gap in K_{IR}2.1 phylogeny. Similar as demonstrated for other turtle genes [35,36], our *Tse*K_{IR}2.1 sequence was more closely related to avian than to snake K_{IR}2.1.

3.5. Functional characterization of *Lg*K_{IR}2.1

Since the snake K_{IR}2.1 is the most distant from mammalian K_{IR}2.1 channel proteins, functional characterization was performed on this channel. *Lg*K_{IR}2.1 was transiently expressed in COS-7 cells and protein lysates were analysed for K_{IR}2.1 expression by western blot. *Lg*K_{IR}2.1 transfected cells revealed a band at a M_w of approximately 55 kDa, similar as seen for human K_{IR}2.1 (Fig. 4A). Upon transient expression in COS-7 cells, immunofluorescence microscopy with aid of an antibody directed against the C-terminus of the channel protein, revealed membrane staining for *Lg*K_{IR}2.1 similar as for human K_{IR}2.1 (Fig. 4B). In addition, intracellular staining was observed, most likely resulting from expression in the endoplasmatic reticulum and Golgi apparatus.

To establish functional characteristics, HEK293 cells were transiently transfected with *Lg*K_{IR}2.1 and subsequently used for single cell patch-clamp measurements. Characteristic barium sensitive K_{IR}2.1 based inward rectifier current profiles were observed (Fig. 4C, D). The barium IC_{50} value was 6.0 ± 0.6 μM (Fig. 4E) which is comparable to mouse K_{IR}2.1 channels expressed in HEK293 cells [37], but four-fold lower than K_{IR}2.1 channels from the rainbow trout expressed in COS-1 cells [23].

Acknowledgments

We would like to acknowledge Siranush Achoyan, Lou-Ella Alexander, Jirre Zelen and Suhela Sharif for their contribution in cloning the open reading frames of the K_{IR}2.1 channels. We acknowledge Marja Kik (Faculty of Veterinary Medicine, Utrecht University), Igor Efimov (Washington Univeristy, St. Louis), John Jansen and Dirk de Jong for providing snake, turtle, black bear, fish and Japanese quail tissue, respectively.

Appendix A. Supplementary data

Supplementary data associated with this article can be found, in the online version, at http://dx.doi.org/10.1016/j.bbrc.2014.09.031.

References

[1] H. Hibino, A. Ananobe, K. Furutani, et al., Inwardly rectifying potassium channels: their structure, function, and physiological roles, Physiol. Rev. 90 (2010) 291–366.
[2] T.P. de Boer, M.J. Houtman, M. Compier, M.A.G. van der Heyden, The mammalian KIR2.x inward rectifier ion channel family: expression pattern and pathophysiology, Acta Physiol. (Oxf) 199 (2010) 243–256.
[3] B.S. Bhoelan, C.H. Stevering, A.T. van der Boog, M.A.G. van der Heyden, Barium toxicity and the role of the potassium inward rectifier current, Clin. Toxicol. (Phila) 52 (2014) 584–593.
[4] N.M. Plaster, R. Tawil, M. Tristani-Firouzi, et al., Mutations in Kir2.1 cause the developmental and episodic electrical phenotypes of Andersen's syndrome, Cell 105 (2001) 511–519.
[5] H.L. Nguyen, G.H. Pieper, R. Wilders, Andersen–Tawil syndrome: clinical and molecular aspects, Int. J. Cardiol. 170 (2013) 1–16.

[6] A. Kuo, J.M. Gulbis, J.F. Antcliff, et al., Crystal structure of the potassium channel KirBac1.1 in the closed state, Science 300 (2003) 1922–1926.
[7] S. Pegan, C. Arrabit, W. Zhou, et al., Cytoplasmic domain structures of Kir2.1 and Kir3.1 show sites for modulating gating and rectification, Nat. Neurosci. 8 (2005) 279–287.
[8] X. Tao, J.L. Avalos, J. Chen, R. MacKinnon, Crystal structure of the eukaryotic strong inward-rectifier K+ channel Kir2.2 at 3.1 Å resolution, Science 326 (2009) 1668–1674.
[9] O.B. Clarke, A.T. Caputo, A.P. Hill, J.I. Vandenberg, B.J. Smith, J.M. Gulbis, Domain reorientation and rotation of an intracellular assembly regulate conduction in Kir potassium channels, Cell 141 (2010) 1018–1029.
[10] S.B. Hansen, X. Tao, R. MacKinnon, Structural basis of PIP2 activation of the classical inward rectifier K+ channel Kir2.2, Nature 477 (2011) 495–498.
[11] V.N. Bavro, R. De Zorzi, M.R. Schmidt, et al., Structure of a KirBac potassium channel with an open bundle crossing indicates a mechanism of channel gating, Nat. Struct. Mol. Biol. 19 (2012) 158–163.
[12] P.J. Stansfeld, R. Hopkinson, F.M. Ashcroft, M.S. Sansom, PIP2-binding site in Kir channels: definition by multiscale biomolecular simulations, Biochemistry 48 (2009) 10926–10933.
[13] F. Khalili-Araghi, J. Gumbart, P.C. Wen, M. Sotomayor, E. Tajkhorshid, K. Schulten, Molecular dynamics simulations of membrane channels and transporters, Curr. Opin. Struct. Biol. 19 (2009) 128–137.
[14] J.L. Robertson, L.G. Palmer, B. Roux, Long-pore electrostatics in inward-rectifier potassium channels, J. Gen. Physiol. 132 (2008) 613–632.
[15] K. Tai, P.J. Stansfeld, M.S. Sansom, Ion-blocking sites of the Kir2.1 channel revealed by multiscale modelling, Biochemistry 48 (2009) 8758–8763.
[16] R. Caballero, P. Dolz-Gaitón, R. Gómez, et al., Flecainide increases Kir2.1 currents by interacting with cysteine 311, decreasing the polyamine-induced rectification, Proc. Natl. Acad. Sci. USA 107 (2010) 15631–15636.
[17] S.F. Noujaim, J.A. Stuckey, D. Ponce-Balbuena, et al., Structural bases for the different anti-fibrillatory effects of chloroquine and quinidine, Cardiovasc. Res. 89 (2011) 862–869.
[18] A. Inanobe, N. Kamiya, S. Murakami, Y. Fukunishi, H. Nakamura, Y. Kurachi, In silico prediction of the chemical block of human ether-a-go-go-related gene (hERG) K+ current, J. Physiol. Sci. 58 (2008) 459–470.
[19] L. Boukharta, H. Keränen, A. Stary-Weinzinger, G. Wallin, B.L. de Groot, J. Aqvist, Computer simulations of structure-activity relationships for HERG channel blockers, Biochemistry 50 (2011) 6146–6156.
[20] M.J. Forster, Molecular modelling in structural biology, Micron 33 (2002) 365–384.
[21] Y. Kubo, T.J. Baldwin, Y.N. Jan, L.Y. Jan, Primary structure and functional expression of a mouse inward rectifier potassium channel, Nature 362 (1993) 127–133.
[22] D.S. Navaratnam, L. Escobar, M. Covarrubias, J.C. Oberholtzer, Permeation properties and differential expression across the auditory receptor epithelium of an inward rectifier K+ channel cloned from the chick inner ear, J. Biol. Chem. 270 (1995) 19238–19245.
[23] M. Hassinen, V. Paajanen, J. Haverinen, H. Eronen, M. Vornanen, Cloning and expression of cardiac Kir2.1 and Kir2.2 channels in thermally acclimated rainbow trout, Am. J. Physiol. Regul. Integr. Comp. Physiol. 292 (2007) R2328–2339.
[24] M.A.G. van der Heyden, B. Kok, E.N. Kouwenhoven, et al., Cloning, sequence analysis and phylogeny of connexin43 isolated from American black bear heart, DNA Seq. 18 (2007) 380–384.
[25] M.A.G. van der Heyden, M. van Eijk, R. Wilders, J.M.T. de Bakker, T. Opthof, Connexin43 orthologues in vertebrates: phylogeny from fish to man, Dev. Genes. Evol. 214 (2004) 261–266.
[26] K. Tamura, J. Dudley, M. Nei, S. Kumar, MEGA4: Molecular Evolutionary Genetics Analysis (MEGA) software version 4.0, Mol. Biol. Evol. 24 (2007) 1596–1599.
[27] J.A. Jansen, T.P. de Boer, R. Wolswinkel, et al., Lysosome mediated Kir2.1 breakdown directly influences inward rectifier current density, Biochem. Biophys. Res. Commun. 367 (2008) 687–692.
[28] M.J.C. Houtman, H. Takanari, B.G. Kok, et al., Experimental mapping of the canine KCNJ2 and KCNJ12 gene structures and functional analysis of the canine KIR2.2 ion channel, Front. Physiol. 3 (2012) 9.
[29] C. Stockklausner, J. Ludwig, J.P. Ruppersberg, N. Klöcker, A sequence motif responsible for ER export and surface expression of Kir2.0 inward rectifier K+ channels, FEBS Lett. 493 (2001) 129–133.
[30] A. Hofherr, B. Fakler, N. Klöcker, Selective Golgi export of Kir2.1 controls the stoichiometry of functional Kir2.x channel heteromers, J. Cell Sci. 118 (2005) 1935–1943.
[31] M. Xia, Q. Jin, S. Bendahhou, et al., A Kir2.1 gain-of-function mutation underlies familial atrial fibrillation, Biochem. Biophys. Res. Commun. 332 (2005) 1012–1019.
[32] N.P. Davies, P. Imbrici, D. Fialho, et al., Andersen–Tawil syndrome: new potassium channel mutations and possible phenotypic variation, Neurology 65 (2005) 1083–1089.
[33] M.M. Limberg, S. Zumhagen, M.F. Netter, et al., Non dominant-negative KCNJ2 gene mutations leading to Andersen–Tawil syndrome with an isolated cardiac phenotype, Basic Res. Cardiol. 108 (2013) 353.
[34] D. Leonoudakis, L.R. Conti, C.M. Radeke, L.M. McGuire, C.A. Vandenberg, A multiprotein trafficking complex composed of SAP97, CASK, Veli, and Mint1 is associated with inward rectifier Kir2 potassium channels, J. Biol. Chem. 279 (2004) 19051–19063.
[35] S.B. Hedges, L. Poling, A molecular phylogeny of reptiles, Science 283 (1999) 998–1001.
[36] Y. Chiari, V. Cahais, N. Galtier, F. Delsuc, Phylogenomic analyses support the position of turtles as the sister group of birds and crocodiles (Archosauria), BMC Biol. 10 (2012) 65.
[37] B.K. Panama, M. McLerie, A.N. Lopatin, Functional consequences of Kir2.1/Kir2.2 subunit heteromerization, Pflugers Arch. 460 (2010) 839–849.